RSC Advances

PAPER

View Article Online
View Journal | View Issue

Cite this: *RSC Adv.*, 2022, **12**, 9069

Synergistically assembled graphene/ZnO composite to enhance anticorrosion performance of waterborne epoxy coatings†

Kuilin Lv, *[ab] Ruina Pan,[a] Lei Zhang,[a] Yuan Tian,[a] Yanqiu Sui[a] and Detian Wan*[ab]

Received 14th February 2022
Accepted 16th March 2022

DOI: 10.1039/d2ra00959e

rsc.li/rsc-advances

In this work, waterborne epoxy resin and graphene/ZnO (Gr/ZnO) were employed as the matrix and nanofiller to construct composite coatings with enhanced anticorrosive performance. The corrosion protection properties of the coatings were significantly improved by the dispersed Gr sheets, as well as the parallelly assembled ZnO nanoparticles. The most remarkable improvement was achieved by adding 0.04 wt% of Gr and 0.4 wt% of ZnO in the Waterborne Epoxy (WEP) coatings, where the highest impedance was 200 530 Ω cm^2 on $Gr_{0.04}$–$ZnO_{0.4}$, far more than pure epoxy with 6186 Ω cm^2 after 7 days of immersion in electrolytes. Furthermore, the $Gr_{0.04}$–$ZnO_{0.4}$ coatings and corresponding corrosion products immersed in a 3.5% NaCl solution for 30 days were also characterized, which could further reveal anticorrosion mechanisms of the graphene modified WEP coatings and the passivated effect of ZnO. Through the mechanism analysis, we also found that ZnO could be employed as the barrier reinforcement to improve the dispersibility of graphene in WEP coatings, and the parallel assembly of graphene occurs spontaneously, leading to remarkable improvement of anticorrosion properties.

1. Introduction

Metallic corrosion generally occurs in the field of construction, marine environments, transportation, aerospace and our daily life. In addition, the personnel safety and economic losses caused by metallic corrosion are continually increasing, which has posed a serious threat to the natural environments and industrial structure.[1–3] However, according to the statistics, the annual global loss resulting from metallic corrosion was more than 2.0 trillion dollars.[4] Thus, it is very necessary to prevent the metal surfaces from coming into contact with corrosive media (such as H_2O, O_2, H^+ and Cl^-), and protect metals against corrosion.[5] Nowadays, the ubiquitous approach for anticorrosion mainly focuses on the development of the surface modification or coatings. Compared with the conventional anticorrosive paints, the waterborne epoxy paints (WEP) have various kinds of advantages, including expediting setting, good mechanical properties, and environmentally ingredient.[6–8] Although the commercial technology of WEP paints is mature, they still suffer from some intrinsic disadvantages, such as decreased shielding ability of vapor diffusion, inferior water-resistant lifetime and poor long-term anticorrosive ability.[9,10] Furthermore, due to the defective coalescence of epoxy particles during the anticorrosive process, there are incomplete particles or surfactants at the interface of WEP coating, which providing a unique mechanism by which the H_2O, O_2, H^+ or Cl^- rapidly penetrate the coatings.[11]

Introducing the nano-additive into WEP coatings is an effective way to solve above disadvantages, such as MoS_2,[12,13] BN,[14] TiO_2,[15–17] graphene oxide (GO)[18] or graphene (Gr).[19] Among them, graphene has attracted much attention due to its excellent physical properties, electrical conductivity, and honeycomb lattice structure by single sp^{2-} bonded C atom.[20] For doping graphene in WEP coatings (Gr/WEP), the well dispersive of graphene nanosheets can form long and tortuous paths which restricts the diffusion of H_2O, O_2, H^+ and Cl^-, thus improving the anticorrosive properties of WEP coatings.[21] For example, Huan *et al.* reported that waterborne epoxy resin E44 and graphene were employed as the matrix and nanofiller to construct composite coatings with enhanced anticorrosive performance.[22] In addition, Li *et al.* fabricated sulfonated graphene (SG) to fill in the WEP coatings by introducing the sulfonic acid groups on graphene sheets and the most remarkable improvement was achieved by adding 1.0 wt% of SG, where the impedance modulus at 0.1 Hz was 193 times higher than the neat WEP coatings after 150 days of immersion.[23] Unfortunately, due to the poor dispersibility in the WEP and excess water dispersible of graphene, which will limit the anticorrosive application of Gr (or other nanomaterials) and even accelerated corrosion on WEP coatings. In other word, direct incorporation of graphene into WEP coatings is not a good strategy since the rapid

[a]*China Testing & Certification International Group Co, Ltd Room, Chaoyang District, Beijing, China. E-mail: lvkuilin@ctc.ac.cn*

[b]*State Key Laboratory of Green Building Materials, China State Building Materials Research Institute Co, Ltd Room, Chaoyang District, Beijing, China*

† Electronic supplementary information (ESI) available. See DOI: 10.1039/d2ra00959e

agglomeration can accelerate corrosion.[24,25] Therefore, an appropriate doping content and the well dispersibility of Gr are conducived to decrease the agglomeration in WEP coatings.

Dispersing nanoparticles in WEP coatings will provide a solution to the failure of single coating. Researchers have added a variety of nanoparticles into the polymer coating to alter its mechanical, optical or chemical properties, which meaning that the choice of nanoparticles can depend on the properties of WEP coating. For example, Fe_2O_3 nanoparticles can be used to improve the magnetic response and corrosion resistance of coatings;[26] The selection of TiO_2 nanoparticles can be used to improve the photo-oxidation stability, self-cleaning and antibacterial properties.[27] In order to improve electrical conductivity and anticorrosion, Al_2O_3 or ZnO nanoparticles were added. In a word, adding these inorganic nano-fillers to the organic coatings can fully reflect the advantages of each component, which effectively reduce or eliminate the shortcomings of each component.[26–28] In addition, nanoparticles can also prevent depolymerization of epoxy resin during curing. When nanoparticles tend to occupy pore defects formed by local shrinkage of WEP, which will act as bridges for intermolecular interconnection, resulting in reduced tendency to more uniform.[9] Among them, it is pointed out that ZnO nanoparticles can be more uniform on the surface of Gr. When the WEP coatings is disturbed or vibrated, ZnO nanoparticles will produce a certain outward expansion tension, which can open Gr sheets into small flakes.[29] Finally, ZnO nanoparticles and Gr can be evenly dispersed in the epoxy resin, which play a better physical barrier effect to improve the anticorrosive performance.

Herein, graphene and ZnO were doped into WEP coatings (denoted as Gr_x–ZnO_y, x and y represent the weight percent of WEP coatings) was synthesis by cost-effective stirring process in the presence of the epoxy resin and water solvent. During the stirring process, graphene has been extensively introduced to polymer coatings, and simultaneously ZnO nanoparticles were uniformly created on the surface and interlayer of graphene. Among them, graphene nanosheets were prepared according to our reported literature.[30] The large-scale graphene nanosheets with a high concentration were directly fabricated from bulk graphene by a facile, cost-efficient and scalable ball-milling method, which provides an opportunity for their practical application. For comparison, different doping content of graphene and ZnO in the WEP coatings were prepared to explore the appropriate doping content. The as-prepared Gr_x–ZnO_y, particularly $Gr_{0.04}$–$ZnO_{0.4}$, which exhibited the highest impedance of 200 530 Ω cm^2 and the lowest corrosion current of 4.15 $\times 10^{-8}$ A cm^{-2} for 7 days immersion in 3.5 wt% NaCl solution. Comparing with pure WEP coatings (Gr_0–ZnO_0) and $Gr_{0.04}$–ZnO_0, the anticorrosion and mechanical properties of $Gr_{0.04}$–$ZnO_{0.4}$ coatings were improved after adding the appropriate 0.04 wt% content of graphene. We also found that ZnO can be employed as the barrier reinforcement and improved the dispersibility of graphene in WEP coatings. When the filler content of ZnO reached 0.4 wt%, the parallel assembly of graphene sheets occurred spontaneously and instead of forming agglomerations, which leading to a remarkable improvement of anticorrosion property.

2. Materials

The exfoliated graphene nanosheets was prepared according to our previous report.[30] Zinc oxide nanoparticles (ZnO, 99.99%) and NaCl (99.9%) were purchased from Guangzhou Zhongwan New Material Co. Ltd. Waterborne epoxy dispersion, waterborne epoxy curing agent, defoamer and cosolvent were purchased from Alfa Aesar. All reagents were used without further treatment. The Q235 steel substrates (size: 0.3 mm × 20 mm × 20 mm) for corrosion study were firstly polished with 500, 1000 and 1500 mesh of abrasive paper, then ultrasonic cleaning in alcohol, and finally dried in air.

2.1 Synthesis of Gr/ZnO composite

Prior to the synthesis of Gr/ZnO composite, and graphene was prepared according to our previous report.[30] Graphene (0.01 g) and ZnO (0.1 g) were well dispersed in H_2O (30 mL) by ultrasonic dispersion for 30 min to prepare Gr/ZnO dispersion. At the end of the reaction, Gr/ZnO was obtained by washing with deionized water for several times by suction filtration and freeze-drying for 12 h.

2.2 Preparation of Gr_x–ZnO_y composite epoxy coatings

Firstly, 0.018 g of graphene and 0.184 g of ZnO nanoparticles were dropped into waterborne epoxy dispersion (30 g) and then stirred for 30 min to produce a homogeneous solution. After that, 0.5 g of defoamer were added into as-prepared solution and then stirred for 30 min to obtain component A. Component B is waterborne epoxy curing agent (polyamide). These two components were mixed with the weight ratio of 2 : 1 (A/B) and stirred at 1500 rpm min^{-1} for 30 min at room temperature. The coatings solidified at room temperature until the surface of the coating was dry, then cured at 60 °C for 12 h to obtain 0.04 wt% of Gr/0.4 wt% of ZnO/epoxy coating, which was named as $Gr_{0.04}$–$ZnO_{0.4}$. $Gr_{0.04}$–$ZnO_{0.4}$ composites were fabricated on the Q235 steel substrates using the wire bar coater (25 μm), and these coatings were naturally cured 48 h at room temperature. For comparison, the pure epoxy coating (Gr_0–ZnO_0), 0.04 wt% of Gr/epoxy coating ($Gr_{0.04}$–ZnO), 0.02 wt% of Gr/0.4 wt% of ZnO/epoxy coating ($Gr_{0.02}$–$ZnO_{0.4}$) and 0.06 wt% of Gr/0.4 wt% of ZnO/epoxy coating ($Gr_{0.02}$–$ZnO_{0.4}$) were also fabricated *via* the same procedures, just only without adding varied content of graphene or ZnO. In addition, we also prepared $Gr_{0.04}$–$ZnO_{0.2}$ and $Gr_{0.04}$–$ZnO_{0.6}$ epoxy coating to explore the influence of adding ZnO content. The compositions of the investigated samples have been added in the revised manuscript (Table S6†).

2.3 Characterizations

The surface morphologies of samples were observed under Field Emission Scanning Electron Microscope (FESEM) (JEOL, JSM-7500F, Japan). Infrared spectroscopy (FTIR) were taken by spectrometer with He–Ne radiation (Thermo Nicolet, NEXUS 670). A optical microscope (KEYENCE, VHX-970F) was used to

evaluate the thickness of the coatings, and we measured three times to take average value. To study the adhesion of coating and substrate, the drawing method was used to determine the interfacial bonding strength. According to the Chinese National Standard GB/T5210-2006 "The pull method adhesion test for paint and varnish". The drawing method for adhesion test refers to the application of vertical and uniform tension to observe the force required for the coating detach from the substrate. The testing machine is single column electronic universal material testing machine (SHIMadzu, EZ-LX).

2.4 Electrochemical measurements

Electrochemical experiments were performed on the electrochemical work station (CHI760E), 0.1 M solution of $KHCO_3$ was used as the electrolyte. The three electrodes system was adopted, in which the working electrode, Ag/AgCl electrode (the saturated KCl solution) and Pt sheet were used as the reference electrode, and the counter electrode, respectively. The Q235 steel with coatings samples was used as the working electrode, and the effective area on Q235 steel of working electrode was 1 cm^2. The electrochemical impedance spectroscopy (EIS) was performed using periodic potential disturbances of 10 mHz to 100 kHz in frequency and 10 mV in amplitude. Before the measurements, the coating samples were immersed in 3.5 wt% NaCl solution. In addition, the Tafel polarization test was carried out with a constant weep rate of 2 mV s^{-1}, the corrosion potential (E_{corr}) and corrosion current density (i_{corr}) were obtained by this method. All electrochemical reductions were conducted for 2 h with a pH value of 6.8 at room temperature. The potentials were recorded *versus* RHE with the conversion, using the formula: E (*vs.* RHE) = E (*vs.* Ag/AgCl) + 0.197V + 0.0591 × pH. Each group of electrochemical experiment was performed more than five times, and until the data of EIS were stabilized.

3. Results and discussion

3.1 Characterization of samples and coatings

The surface morphologies of samples and coatings are observed by scanning electron microscope (SEM) (Fig. 1). From the local magnification of (b1 and b2), it can be seen that there are holes in the mixed film, which mainly due to the agglomeration of graphene. During the mixing and preparation of materials in the early stage, the lamellar structure of graphene is not fully demonstrated, and its physical barrier properties cannot be fully utilized in an efficient manner. As a result, microscopic defects appear in the film scraping of Gr_0–$ZnO_{0.4}$ coating, and the fatal defects appear in the anticorrosive coating for the later stage. But at the same time, compared with the sectional drawing of Gr_0–ZnO_0 coating, $Gr_{0.04}$–ZnO_0 was much compact than Gr_0–ZnO_0, as the figure of the magnified images (a1 and b1). This means that graphene could be inserted into the epoxy coating, which increasing the thickness of the coating and eliminating the porous interior of the film. But when 0.4 wt% ZnO particles were added, compared with Gr_0–ZnO_0 and $Gr_{0.04}$–ZnO_0, the cross section of $Gr_{0.04}$–$ZnO_{0.4}$ coating became more dense (c1 and c2). These results due to the existence of ZnO nanoparticles, so that the modified Gr could not be agglomerated. Gr–ZnO were also well dispersed in epoxy resin, which making wafers compact and multilayers in the $Gr_{0.04}$–$ZnO_{0.4}$. There were two main reasons for the analysis: (1) the nano-effect of materials and the excellent dispersion effect of graphene and ZnO, which can enhance the interfacial bonding strength with epoxy resin and facilitate the stress transfer. (2) When the substrate is impacted by the external environment, microcracks occur between particles and substrate, so that the corrosive medium on the EP is transferred to the nanoparticles through the interface, so that more impact energy is absorbed and the impact resistance are significantly improved.

The few-layer exfoliated graphene had a lamellar structure without obvious agglomeration, and its surface was flat and smooth (Fig. S1†). And the Fig. S1a† shows the SEM images of the as-synthesized Gr/ZnO sample, in which the petaloid ZnO nanoparticles are uniformly distributed in the surface of graphene, thus graphene offer large surface areas for supporting ZnO nanoparticles. The addition of ZnO nanoparticles did not only change the lamellar structure of graphene, but also enhanced the dispersion of layer. In addition, Zn^+ could react with the active site of graphene layer by solution diffusion, which contributing to the better distribution of ZnO nanoparticles and the higher specific surface area of Gr/ZnO. In addition, a optical microscope was used to evaluate the thickness of the coatings, and we measured three times to take average value. As shown in Fig. S2,† the thickness of $Gr_{0.04}$–$ZnO_{0.4}$ coatings was 25 ± 2, which was consistent with the result of using wire bar coaters (25 μm).

The molecular structure of coatings were analysed by infrared spectroscopy (FTIR). As the Fig. 2a of the Gr/ZnO sample, the characteristic absorption peak of 499 cm^{-1}, 1080 cm^{-1}, 1636 cm^{-1} and 3413 cm^{-1} were ZnO, C–O, Zn–O and O–H, respectively, thus indicating ZnO nanoparticles are distributed in the interspace of graphene layers. As for Gr_0–ZnO_0, these peaks around 1030–1080 cm^{-1}, 1616 cm^{-1}, 2900 cm^{-1} and 3400 cm^{-1} can be indexed to the C–O, C=C, C–H and O–H absorption peak of pristine EP coating.[18] Comparing the FTIR patterns of the Gr_0–ZnO_0 and $Gr_{0.04}$–$ZnO_{0.4}$ (Fig. 2b and c), we found that the Zn–O diffraction peaks of $Gr_{0.04}$–$ZnO_{0.4}$ was obviously appeared at 1636 cm^{-1}, indicating that graphene layers/ZnO nanoparticles were successfully doped and stable existed in EP coating.

3.2 Electrochemical properties of GEP coatings

Tafel polarization curves of five kinds of coatings were shown in Fig. 3a. The specific data of electrochemical measurements (*i.e.* corrosion potential (E_{corr}), corrosion current (i_{corr}) and corrosion rate (η) measured in 3.5 wt% aqueous NaCl electrolyte) for one week were listed in Table S1.† Information about E_{corr} and i_{corr} can be obtained by the point of intersection of cathodic and anodic polarization curves. In general, when the value of E_{corr} is larger or i_{corr} is smaller, which indicates that the corrosion resistance of coating is better.[20] For the pristine EP (Gr_0–ZnO_0) coating, its corrosive potential and current are −631.36 mV and

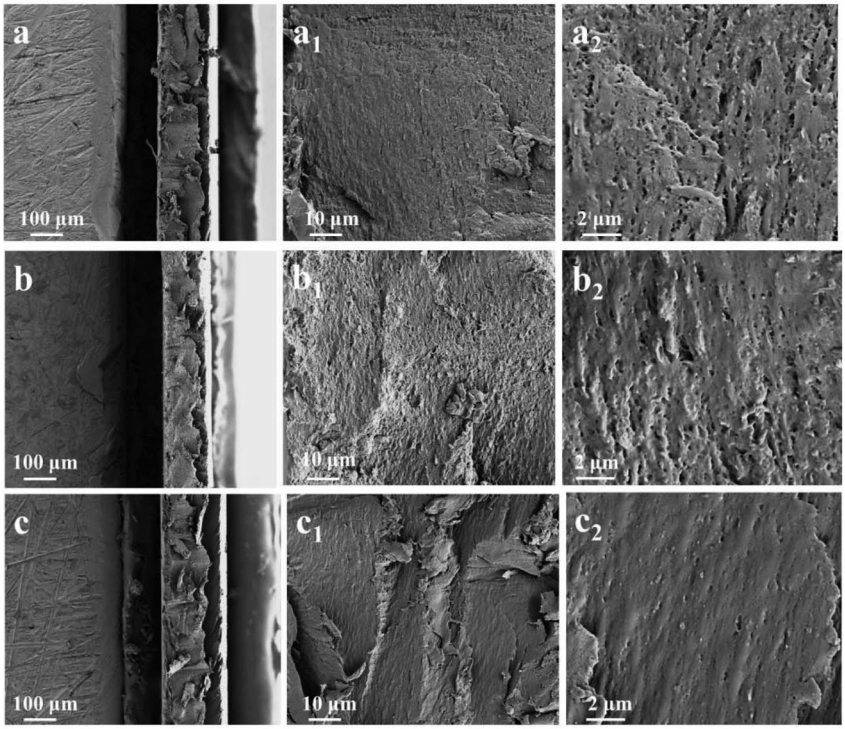

Fig. 1 The fracture surface SEM of Gr_0–ZnO_0 coating (a), $Gr_{0.04}$–ZnO_0 coating (b), $Gr_{0.04}$–$ZnO_{0.4}$ coating (c).

9.40×10^{-6} A cm^{-2}, respectively. And there were many micropores and microcracks on the surface or interior of Gr_0–ZnO_0, so H_2O and O_2 could diffuse through these mic-channels to the metallic surface, resulting in poorer anticorrosion.[12] The Tafel polarization curves of different Gr_x–ZnO_y coatings are displayed in Fig. 3a, as the graphene addition amount increases, the E_{corr} increases and the i_{corr} decreases. But when 0.04 wt% graphene is added, the E_{corr} increased with increasing graphene content and reached a maximum of −527.80 mV on $Gr_{0.04}$–$ZnO_{0.4}$, larger than those for E_{corr} on Gr_0–ZnO_0 (−631.36 mV), $Gr_{0.02}$–$ZnO_{0.4}$ (−599.13 mV) and $Gr_{0.06}$–$ZnO_{0.4}$ (−560.74 mV), which showing outstanding anticorrosion property. For comparison, Fig. 4a also showed the Tafel polarization curves of $Gr_{0.04}$–ZnO_0, $Gr_{0.04}$–$ZnO_{0.1}$, $Gr_{0.04}$–$ZnO_{0.4}$ and $Gr_{0.04}$–ZnO_1 by the different ZnO content. And the highest E_{corr} or the lowest i_{corr} was appeared on $Gr_{0.04}$–$ZnO_{0.4}$ among them (Table S2†), which indicated that the best corrosion resistance of $Gr_{0.04}$–$ZnO_{0.4}$ for the moderately doping Gr and ZnO. When graphene and ZnO were added into the pristine EP coatings, these micropores could be occupied and the diffusion of H_2O and O_2 could also be effectively inhibited, so the electrochemical reactions could be decreased and thus the corrosive current decreased. Due to ZnO nanoparticles were adsorbed in the gap between Gr and EP, which reducing the chance of oxygen entering the coating interior and also increasing the corrosion path.

In addition, the EIS technique is another electrochemical way to evaluate the anticorrosion nature of organic coatings. In this work, the impedance spectra of Gr_x–ZnO_x coatings were measured in 3.5 wt% NaCl solution at room temperature. The Nyquist plots of Gr_0–ZnO_0, $Gr_{0.04}$–ZnO_0, $Gr_{0.02}$–$ZnO_{0.4}$, $Gr_{0.04}$–

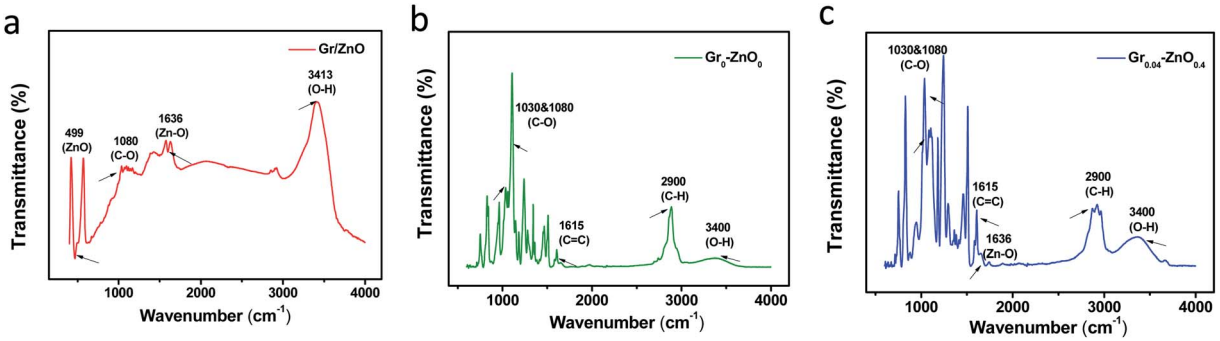

Fig. 2 FTIR spectra of Gr/ZnO (a), Gr_0–ZnO_0 (b), and $Gr_{0.04}$–$ZnO_{0.4}$ (c) coatings.

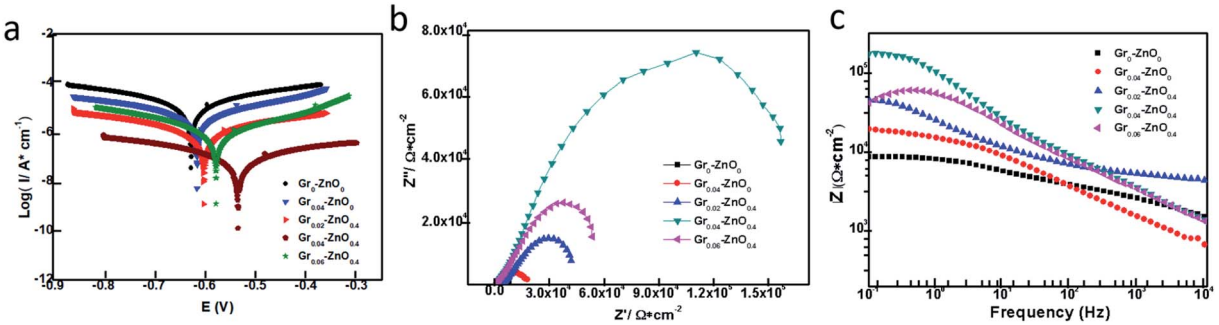

Fig. 3 After 1 week of immersion, (a), (b) and (c) are the Tafel image, Nyquist plots and Bode modulus plots of different EP coatings, respectively.

$ZnO_{0.4}$ and $Gr_{0.06}$–$ZnO_{0.4}$ coatings as shown in Fig. 3b, which clearly indicated that the $Gr_{0.04}$–$ZnO_{0.4}$ coatings shows the largest impedance arc among these coatings. For comparison, the Nyquist plots of $Gr_{0.04}$–ZnO_0, $Gr_{0.04}$–$ZnO_{0.1}$, $Gr_{0.04}$–$ZnO_{0.4}$ and $Gr_{0.04}$–ZnO_1 coatings by the different ZnO contents as shown in Fig. S3† clearly indicated that the sample $Gr_{0.04}$–$ZnO_{0.4}$ shows the largest impedance among these coatings. And Tables S3 and S4† also implied that $Gr_{0.04}$–$ZnO_{0.4}$ has greater electrochemical impedance (200 530 Ω cm^2) than Gr_0–ZnO_0 (6186 Ω cm^2), $Gr_{0.02}$–$ZnO_{0.4}$ (42 096 Ω cm^2) and $Gr_{0.06}$–$ZnO_{0.4}$ (56 695 Ω cm^2) coatings. Thus, the anticorrosion property of waterborne epoxy resin coating was enhanced by the appropriate addition of Gr. When the 0.04 wt% of Gr and 0.4 wt% of ZnO were used as the nano-filler in pristine EP coating, a few micropores could be occupied and the diffusion pathway of corrosive media could be hold back, so the anticorrosion property of waterborne epoxy-based coating was enhanced. The EIS data (Tables S3 and S4†) was analyzed and obtained by ZSimpWin software. As the figure, Gr_0–ZnO_0, $Gr_{0.04}$–ZnO_0, $Gr_{0.02}$–$ZnO_{0.4}$, $Gr_{0.04}$–$ZnO_{0.4}$ and $Gr_{0.06}$–$ZnO_{0.4}$ all have only one time constant, which indicates that the coating corrosion is still in the stage of electron transfer. And the equivalent circuit in Fig. S5† can fit the EIS data with only one time constant, where R_s represents the solution resistance, R_p represents coating resistance, C represents coating capacitance. In addition, Y_0 and n are admittance and empirical constants, respectively. The value of n is $0 \leq n \leq 1$, which is related to the roughness and homogeneity of the coating. When the value of n closes to 1, the constant phase element tends to be pure electricity. On the contrary, the coating approximates pure resistance as the value of n approaches 0. Combined with Table S3† and Fig. 3b, the Nyquist curve of Gr_0–ZnO_0 shows the characteristic of cross current impedance from charge transfer to diffusion process, because the coating structure is not dense enough and the corrosive medium penetrates the coating and contacts the substrate. For comparison, it can be seen that the R_p and C value of $Gr_{0.04}$–$ZnO_{0.4}$ is the largest, indicating that the optimized coating is the most dense and can more effectively prevent the corrosive medium from infiltrating into the metal matrix.

The Bode modulus plots of different content of Gr–$ZnO_{0.4}$ coatings are also displayed in Fig. 3c. The value of Bode modulus ($f = 0.01$ Hz) is an another important electrochemical parameter to evaluate the anticorrosion property of coatings, and the higher Bode modulus exhibites the better anticorrosion performance.[19] The low frequency impedance (Log $|Z|$) of the pristine EP coating was not exceed 10^4 Ω cm^2, but the coating containing Gr/ZnO for Log $|Z|$ were all more than 10^4 Ω cm^2. In particular, the Log $|Z|$ of $Gr_{0.04}$–$ZnO_{0.4}$ was greater than 10^5 Ω

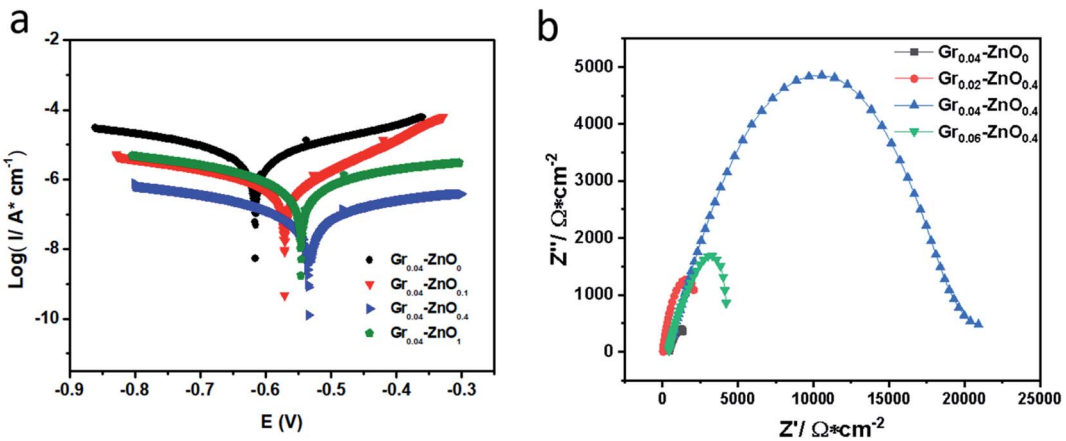

Fig. 4 (a) After 1 week of immersion, the Tafel image of $Gr_{0.04}$–ZnO_0, $Gr_{0.04}$–$ZnO_{0.1}$, $Gr_{0.04}$–$ZnO_{0.4}$ and $Gr_{0.04}$–ZnO_1. (b) After one month of immersion, the electrochemical impedance of $Gr_{0.04}$–ZnO_0, $Gr_{0.02}$–$ZnO_{0.4}$, $Gr_{0.04}$–$ZnO_{0.4}$ and $Gr_{0.06}$–$ZnO_{0.4}$.

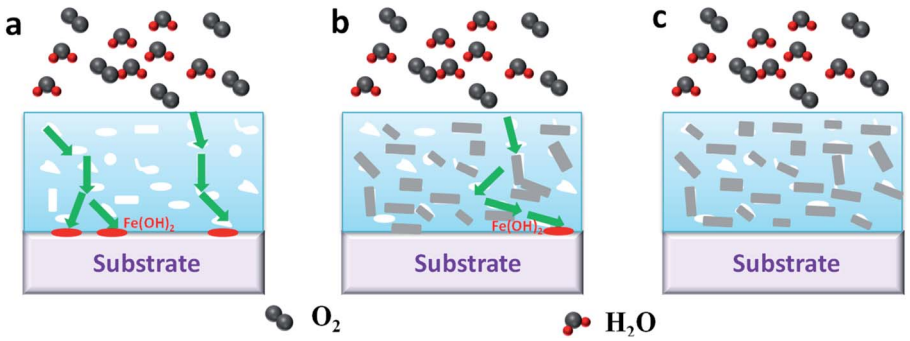

Fig. 5 Schematic diagram on the enhanced anticorrosive mechanism. (a), (b), (c) are Gr_0–ZnO_0 coatings, $Gr_{0.04}$–ZnO_0 coatings and $Gr_{0.04}$–$ZnO_{0.4}$ coatings, respectively.

cm^2, which reached the highest in all samples and exhibited better anticorrosion performance. Fig. S4† also showed the Bode modulus plots of $Gr_{0.04}$–ZnO_0, $Gr_{0.04}$–$ZnO_{0.1}$, $Gr_{0.04}$–$ZnO_{0.4}$ and $Gr_{0.04}$–ZnO_1 by the different contents of ZnO. And the Log $|Z|$ of $Gr_{0.04}$–$ZnO_{0.4}$ also the largest than $Gr_{0.04}$–ZnO_0, $Gr_{0.04}$–$ZnO_{0.1}$ and $Gr_{0.04}$–ZnO_1, which had the best anticorrosion property among these samples, in accordance with the analysis of Nyquist plots and Bode modulus plots. In addition, the corrosion resistance for one month of immersion was presented in Fig. 4b. The electrochemical impedance of $Gr_{0.04}$–$ZnO_{0.4}$ was about 200 530 Ω cm^2 at the beginning and gradually decreased to 21 068 Ω cm^2 after 30 days of immersion duration, which was also far better than $Gr_{0.4}$–ZnO_0 (1430 Ω cm^2), $Gr_{0.02}$–$ZnO_{0.4}$ (2202 Ω cm^2) and $Gr_{0.06}$–$ZnO_{0.4}$ (4190 Ω cm^2) coatings. Moreover, it seems that 0.04 wt% of Gr and 0.4 wt% of ZnO content was enough to form the barrier network in the composite WEP coatings. The barrier network formation can be regarded as a percolation phenomenon and the critical filler content is the percolation threshold. The corrosion resistance of WEP coatings becomes worse once the filler content exceeds the percolation threshold. In addition, the typical Nyquist and Bode diagram were added as the Fig. S6 and S7† by ZSimpWin software, which demonstrating a negligible error between the experimental data and the fitting data.

To assess the corrosion resistance of substrates with different coatings in a simulated seawater environment, the bare Q235, Gr_0–ZnO_0, $Gr_{0.04}$–ZNO_0, $Gr_{0.02}$–$ZnO_{0.4}$, $Gr_{0.04}$–$ZnO_{0.4}$ and $Gr_{0.06}$–$ZnO_{0.4}$ were immersed in 3.5 wt% NaCl for accelerated corrosion test at room temperature (Fig. S8†). At the initial stage of 1 day immersion, the surface of the bare Q235 had more obviously passivated layer, and it can also be seen that Gr_0–ZnO_0, $Gr_{0.04}$–ZnO_0, $Gr_{0.02}$–$ZnO_{0.4}$, $Gr_{0.04}$–$ZnO_{0.4}$ and $Gr_{0.06}$–$ZnO_{0.4}$ all had corrosion resistance to substrate. However, after soaking for 1 week, Gr_0–ZnO_0 coating had been completely peeled off. And blisters, cracks and rust appeared on the edges of $Gr_{0.04}$–ZnO_0, rust stains gradually spread to the center with the increase of soaking time. Even after 2 weeks, the lower half of Gr_0–ZnO_0 coating was removed from the substrate, which mean that the substrate lose its protective layer and thus produced yellow porous Fe_2O_3 products. Compared with bare Q235 steel and Gr_0–ZnO_0, $Gr_{0.04}$–$ZnO_{0.4}$ sample were still stable without obvious rust spots and peeling after soaking for 1 month. In addition, Fig. S9† also provides the interfacial bonding strength of different GEP coatings, and $Gr_{0.04}$–$ZnO_{0.4}$ presents a largest interfacial bonding strength of 7.77 Mpa, which is far better than Gr_0–ZnO_0 (2.89 Mpa). These phenomenon is consistent with the results of electrochemical tests, which is attributed to the good dispersion of Gr/ZnO composite in the coating and the physical barrier effect. In addition, these nano-scale particles can be inserted in the micropores of coating, then more corrosive media are blocked on the surface. As listed in Table S5,† although different graphene derivatives were added with different filler content, our materials ($Gr_{0.04}$–$ZnO_{0.4}$) offered the highest anticorrosion properties with the longest immersion duration and the smallest filler content.[22,31–34]

3.3 Enhanced anticorrosive mechanism of $Gr_{0.04}$–$ZnO_{0.4}$ coatings

Based on the results obtained in this work, the enhanced anticorrosive mechanism of the synergistic effect for graphene and ZnO in EP coatings is illustrated in Fig. 5. Since large numbers of micropores and microcracks could be formed inside the EP coating during its curing process, the corrosive media like H_2O, O_2, H^+ or Cl^- could easily permeate through these micropores and microcracks into the interface between EP coating and metallic surface, where the electrochemical corrosion reactions could easily happen on the metallic surface. The electrochemical corrosion reactions can be described as follow:[21] (1) oxidation reaction: $2Fe \rightarrow 2Fe^{2+} + 4e^-$; (2) reduction reaction: $2H_2O + O_2 + 4e^- \rightarrow 4OH^-$; (3) $Fe^{2+} + 2OH^- \rightarrow Fe(OH)_2$. If one of (1) or (2) reactions was inhibited, the overall redox would be suppressed. In addition, it is well known that O_2 and H_2O are requisite for the corrosion reactions, and if O_2 and H_2O were impeded to the interface of EP coating and metal, the corrosion reactions would be prevent and the metallic surface was protected. As shown in Fig. 5b, when the right amount of graphene was added into the EP coating, the micropores and microcracks could be occupied and the permeation of corrosive media would be hindered. Compared with the primary EP coating, the electrochemical reactions of corrosion were more slow, and the

corrosion path would become longer. Accordingly, graphene cannot be completely dispersed in the EP coating, and a few micropores or microcracks would exposed to form a corrosive path. However, when ZnO nanoparticles and graphene were added into WEP coatings (Fig. S10†), the value of contact angle increased from 43.5 ± 3° recorded for the unfilled WEP to 77.6 ± 2° ($Gr_{0.04}$–ZnO_0 sample) to 87.1 ± 2° ($Gr_{0.04}$–$ZnO_{0.4}$ sample). This rise seems to be linked to the quantity of nanofiffiller (Gr/ZnO) contained in the resin; in fact, the contact angle increased as more filler was added, which conferring to the surface a slightly higher hydrophobicity and improving the anticorrosive performance. In addition, due to the exfoliated graphene had more good electrical conductivity, the electrons generated by the oxidation reaction could be quickly migrated from the corrosive sites and thus the corrosion reactions would be decelerated. Consequently, the addition of graphene and ZnO nanoparticles could enhance the anticorrosive performance of waterborne EP coating, which might be attributed to three factors: (i) high surface area and superior dispersion of graphene in the EP coating, (ii) good electrical conductivity of small flakes graphene, and (iii) the better physical barrier effect of graphene and ZnO. In this work, few-layer ZnO/graphene with high surface area was synthesized and collectively employed as the nanofiller in EP coating. Thus, the micropores and microcracks in the EP coating could be fully occupied by these nanofiller, effectively blocking the intrusion of corrosive media.

4. Conclusions

The synergistically assembled of graphene and ZnO were filled in the WEP coatings to improve the corrosion protection properties of WEP. The previous exfoliated graphene sheets can be stably dispersed in both water and WEP emulsions, which caused the demulsification of WEP. After doping ZnO nanoparticles, which did not only enhance the dispersion of layer, but also play a better physical barrier effect for anticorrosive process. With low graphene content of 0.02–0.06 wt%, the graphene sheets presented a single-layer dispersion state. Both well-dispersion and synergistically assembled Gr/ZnO sheets can improve the corrosion protection properties, the most remarkable improvement was achieved because the large number of Gr/ZnO sheets blocked the penetration of electrolytes. Comparing with Gr_0–ZnO_0 (6186 Ω cm^2) and $Gr_{0.04}$–ZnO_0 (19 560 Ω cm^2), the anticorrosive properties of $Gr_{0.04}$–$ZnO_{0.4}$ coatings were both obviously improved, which exhibited the highest impedance of 200 530 Ω cm^2 and the lowest corrosion current of 4.15×10^{-8} A cm^{-2} for 7 days immersion in 3.5 wt% NaCl solution. Through the mechanism analysis, we also found that ZnO can be employed as the barrier reinforcement to improve the dispersibility of graphene in WEP coatings, which leading to a remarkable improvement of anticorrosion property.

Conflicts of interest

There are no conflicts to declare.

Acknowledgements

This work was financially supported by National Natural Science Foundation of China under Grant no. 52102119, National Natural Science Foundation of China under Grant no. 52032011, and China Research Institute of Building Materials Science of Frontier Exploration Foundation program (ZD-11).

References

1 H. W. Huang, M. L. Li, Y. Q. Tian, *et al.*, Exfoliation and functionalization of α-zirconium phosphate in one pot for waterborne epoxy coatings with enhanced anticorrosion performance, *Prog. Org. Coat.*, 2020, **138**, 105390.
2 X. X. Sheng, R. B. Mo, Y. Ma, *et al.*, Waterborne epoxy resin/polydopamine modified zirconium phosphate nanocomposite for anticorrosive coating, *Ind. Eng. Chem. Res.*, 2019, **58**, 16571–16580.
3 M. Irfan, S. I. Bhat, S. Ahmad, *et al.*, Reduced graphene oxide reinforced waterborne soy alkyd nanocomposites: formulation, characterization, and corrosion inhibition. analysis, *ACS Sustainable Chem. Eng.*, 2018, **6**, 14820–14830.
4 J. Ding, H. Zhao, Z. Shao, *et al.*, Bioinspired smart anticorrosive coatings with an emergency-response closing function, *ACS Appl. Mater. Inter.*, 2019, **11**, 42646–42653.
5 X. Luo, J. Zhong, Q. Zhou, *et al.*, Cationic reduced graphene oxide as self-aligned nanofiffiller in the epoxy nanocomposite coating with excellent anticorrosive performance and its high antibacterial activity, *ACS Appl. Mater. Inter.*, 2018, **10**, 18400–18415.
6 S. Liu, L. Gu, H. Zhao, *et al.*, Corrosion resistance of graphene reinforced waterborne epoxy coatings, *J. Mater. Sci. Technol.*, 2016, **32**, 425–431.
7 M. Bagherzadeh, F. Mahdavi, M. Ghasemi, *et al.*, Using Nanoemeraldine Salt-Polyaniline for preparation of a new anticorrosive water based epoxy coating, *Prog. Org. Coat.*, 2010, **68**, 319–322.
8 B. Pang, Y. Zhang, G. Liu, *et al.*, Interface properties of nanosilica-modified waterborne epoxy cement repairing system, *ACS Appl. Mater. Inter.*, 2018, **10**, 21696–21711.
9 F. Zhang, C. Zhang, L. Song, *et al.*, Fabrication of the super hydrophobic surface on magnesium alloy and its corrosion resistance, *J. Mater. Sci. Technol.*, 2015, **31**, 1139–1143.
10 J. Genzer and K. Efifimenko, Recent developments in superhydrophobic surfaces and their relevance to marine fouling: a review, *Biofouling*, 2006, **22**, 339–360.
11 Z. Zhang, T. Zhang, X. Zhang, *et al.*, Mechanically stable superhydrophobic polymer films by a simple hot press lamination and peeling process, *RSC Adv.*, 2016, **6**, 12530–12536.
12 M. Conradi, A. Kocijan, D. Kek-Merl, *et al.*, Mechanical and anticorrosion properties of nanosilica-filled epoxy-resin composite coatings, *Appl. Surf. Sci.*, 2014, **292**, 432–437.
13 T. Simovich, A. H. Wu, R. N. Lamb, *et al.*, Hierarchically Rough, Mechanically Durable and Superhydrophobic Epoxy Coatings through Rapid Evaporation Spray Method, *Thin Solid Films*, 2015, **589**, 472–478.

14 M. Cui, S. Ren, J. Chen, *et al.*, Anticorrosive performance of waterborne epoxy coatings containing water-dispersible hexagonal boron nitride (h-BN) nanosheets, *Appl. Surf. Sci.*, 2016, **397**, 77–86.

15 N. Wang, W. Fu, J. Zhang, *et al.*, Corrosion performance of waterborne epoxy coatings containing polyethylenimine treated Mesoporous-TiO_2 nanoparticles on mild steel, *Prog. Org. Coat.*, 2015, **89**, 114–122.

16 N. Wang, W. Fu, M. Sun, *et al.*, Effect of diffffferent structured TiO_2 particle on anticorrosion properties of waterborne epoxy coatings, *Corros. Eng. Sci. Techn.*, 2016, **51 5**, 365–372.

17 N. Wang, X. Diao, J. Zhang, *et al.*, Corrosion resistance of waterborne epoxy coatings by incorporation of dopamine treated Mesoporous-TiO_2 particles, *Coatings*, 2018, **8**, 209–221.

18 M. Cui, S. Ren, H. Zhao, *et al.*, Polydopamine coated graphene oxide for anticorrosive reinforcement of waterborne epoxy coating, *Chem. Eng. J.*, 2018, **335**, 255–266.

19 R. Ding, Y. Zheng, H. Yu, *et al.*, Study of water permeation dynamics and anti-corrosion mechanism of Graphene/Zinc coatings, *J. Alloys Compd.*, 2018, **748**, 481–495.

20 Z. Chao, H. Shu, W. Weng, *et al.*, Facile preparation of water-dispersible graphene sheets stabilized by acid-treated multi-walled carbon nanotubes and their poly(vinyl alcohol) composites, *J. Mater. Chem.*, 2012, **22**, 2427–2434.

21 H. Shuan, J. Zhao, H. Chen, *et al.*, Corrosion resistance of graphene-reinforced waterborne epoxy coatings, *J. Mater. Sci. Technol.*, 2016, **32**, 425–431.

22 Y. Huan, L. Dan, X. Han, *et al.*, Graphene-induced enhanced anticorrosion performance of waterborne epoxy resin coating, *Front. Mater. Sci.*, 2020, **14**, 211–220.

23 Z. Li, J. Li, J. Cui, *et al.*, Dispersion and parallel assembly of sulfonated graphene in waterborne epoxy anticorrosion coatings, *J Mater. Chem. A.*, 2019, **7**, 17937–17946.

24 Z. Yu, H. Di, Y. Ma, *et al.*, Fabrication of graphene oxide-alumina hybrids to reinforce the anti-corrosion performance of composite epoxy coatings, *Appl. Surf. SCI*, 2015, **351**, 986–996.

25 G. Zhu, X. Cui, Y. Zhang, *et al.*, Poly (vinyl butyral)/graphene oxide/poly (methylhydrosiloxane) nanocomposite coating for improved aluminum alloy anticorrosion, *Polymer*, 2019, **172**, 415–422.

26 L. Vovchenko, O. Lazarenko, *et al.*, Mechanical and electrical properties of the epoxy composites with graphite nanoplatelets and carbon nanotubes, *Phys. Status. Solidi.*, 2014, **211**, 336–441.

27 Z. Li, R. J. Young, R. Wang, *et al.*, The role of functional groups on graphene oxide in epoxy nanocomposites, *Polymer*, 2013, **54**, 5821–5830.

28 Z. Xiong, L. L. Zhang, J. Ma, *et al.*, Photocatalytic degradation of dyes over graphene–gold nanocomposites under visible light irradiation, *Chem. Commun.*, 2010, **46**, 6099–6101.

29 R. Sun, N. Yu, J. Zhao, *et al.*, Chemically stable superhydrophobic polyurethane sponge coated with ZnO/epoxy resin coating for effective oil/water separation, *Chem. Eng. J.*, 2019, **368**, 261–272.

30 C. Teng, D. Xie, J. Wang, *et al.*, Ultrahigh Conductive Graphene Paper Based on Ball-Milling Exfoliated Graphene, *Adv. Funct. Mater.*, 2017, **27**, 20.

31 J. Ding, O. u. Rahman, W. H. Peng, *et al.*, A novel hydroxyl epoxy phosphate monomer enhancing the anticorrosive performance of waterborne Graphene/Epoxy coatings, *Appl. Surf. Sci.*, 2018, **427**, 981–991.

32 L. Gu, S. Liu, H. Zhao, *et al.*, Facile Preparation of Water-Dispersible Graphene Sheets Stabilized by Carboxylated Oligoanilines and Their Anticorrosion Coatings, *ACS Appl. Mater. Interfaces*, 2015, **7**, 17641–17648.

33 S. Liu, L. Gu, H. Zhao, *et al.*, Corrosion Resistance of Graphene-Reinforced Waterborne Epoxy Coatings, *J. Mater. Sci. Technol.*, 2016, **32**, 425–431.

34 S. Wang, Z. Hu, J. Shi, *et al.*, Green synthesis of graphene with the assistance of modified lignin and its application in anticorrosive waterborne epoxy coatings, *Appl. Surf. Sci.*, 2019, **484**, 759–770.